Heliyon 9 (2023) e20261

Contents lists available at ScienceDirect

Heliyon

journal homepage: www.cell.com/heliyon

Solvothermally designed Pr-MOF/Fe_2O_3 based nanocomposites for efficient electrocatalytic water splitting

Bushra Shabbir [a], Karam Jabbour [b], Sumaira Manzoor [a], Muhammad Faheem Ashiq [a], Khaled Fahmi Fawy [c], Muhammad Naeem Ashiq [a,*]

[a] Institute of Chemical Sciences, Bahauddin Zakariya University, Multan, 60800, Pakistan
[b] College of Engineering and Technology, American University of the Middle East, Kuwait
[c] Department of Chemistry, Faculty of Science, King Khalid University, P.O. Box 9004, Abha, 61413, Saudi Arabia

ARTICLE INFO

Keywords:
OER
Composite
MOF
Mechanism

ABSTRACT

To meet the energy demand of modern civilization, efforts to find renewable, safe, and highly effective fuel generation are still a big challenge. The oxygen evolution reaction (OER) is one of many modern technologies for hydrogen generation, and a number of new electrode materials have been created to increase the effectiveness of O_2 evolution. This project utilizes a range of high performance nanomaterials, such as Pr-MOF, Fe_2O_3, and Pr-MOF/Fe_2O_3, to carry out the oxygen evolution reaction. This study shows that Pr-MOF/Fe_2O_3 exhibits exceptional electrocatalytic activity in alkaline solution with 238 mV overpotential at the current density of 10 mA cm^{-2} and a Tafel slope of 37 mV dec^{-1} which is much lower when compared to pure Pr-MOF and Fe_2O_3. The enhanced electrochemical results are due to the higher electrochemical surface area of 237 cm^2. This work will lay the foundation for an approach to enhance the crystalline nature of surface-active nanoparticles made from rare earth MOFs for a range of electrochemical energy applications.

1. Introduction

Every nation looks for a unique energy source to advance its economy and keep up with the trends [1–3]. Finding a strong, long-lasting fuel for earthly life is the primary goal of the current investigation. Owing to their scarcity and the pollution they caused when used to generate electricity for homes and automobiles fossil fuels were less valuable [4]. Due to these difficulties, the research community made the decision to concentrate on novel, renewable energy resources rather than traditional, unsafe fossil fuels [5]. Sustainable energy produced from various sources such as sunlight, wind, tidal, hydroelectric, and geothermal resources has not produced effective result [6]. Numerous studies on recent fuels have shown that hydrogen (H_2), an efficient and environmental friendly fuel, performs substantially better than liquid fuel in terms of availability and efficiency. There were other H_2 possible sources, but water electrolysis emerged as the most active and likely one [7–9]. Water electrolysis contains two half reactions i.e. oxygen evolution reaction (OER) and Hydrogen evolution reaction (HER).

Basically, oxygen evolution reaction (OER) refers to the simultaneous oxidation of H_2O or OH^- ions at the surface of electrode materials and the formation of O_2 gas [10]. RuO_2/IrO_2 and Pt-based nanomaterials have been the most widely used OER electrode material up to this point, and both can accelerate the slow electrocatalytic kinetics at the cathode [11]. However, due to their

* Corresponding author.
E-mail address: naeembzu@bzu.edu.pk (M.N. Ashiq).

https://doi.org/10.1016/j.heliyon.2023.e20261
Received 11 June 2023; Received in revised form 24 August 2023; Accepted 17 September 2023
Available online 22 September 2023

expensive price and low chemical stability, these catalysts' practical and sustainable uses are seriously limited. Additionally, they cannot induce both OER and oxygen reduction reaction (ORR) using a single noble metal catalyst [12–14]. As an alternative for conventional electrocatalysts, the synthesis of non-precious metal materials with improved OER efficiency, reasonable prices, and long term stability durability has attracted a lot of interest [15–17].

Up to now, significant study has been conducted on transition metal-oxide (TMOs), chalcogenides, oxy-hydroxides, sulphides, phosphides and nitrides [18–20]. Even though these efficient electrocatalyst have achieved quicker OER rates, the task is still difficult [21,22]. Metal organic framework (MOFs) can be employed effectively as electrocatalyst for batteries and supercapacitors owing to their unique characteristics, including their significant binding area, tunable pore diameters, low densities, superior thermal stability, and organised crystal structures [23,24]. They also show promise for oxygen evolution reaction (OER) performance [25,26]. But Metal organic framework (MOFs) usually exhibit low resistance to electricity and poor endurance, which lowers the effectiveness of their storage and conversion of energy [27,28]. It's significant that MOFs are used as sacrifice templates to construct various porous nanomaterials with strong electrical properties and electrical reactivity, enabling real world uses for MOF nanostructures [29,30]. The materials that will be used in MOF structures include those based on carbon nanotubes (CNTs), graphene, chalcogenides, various metals, transition metal oxides (TMOs), and porous carbon [31,32].

It is commonly believed that a suitable strategy to reveal the electrochemical efficiency of MOF structures is to introduce a selected conductive active specie into such frameworks [33,34]. Fe_2O_3 interface is one of the ideal nanoscale building units with suitable surface of the catalyst for the creation of composite products due to its aforementioned active nature [35,36]. A fabricated nanocomposite is formed as a result of the relationship between the MOF nanostructure's core positively charged region and the oxygen-containing material Fe_2O_3 [37,38]. Increased permeability of reactant molecules would occur from the interaction of the Fe_2O_3 and MOF nanostructures, which would provide a porous structure along the borders in which the two components interact with one another [39,40]. These newly created active sites would enhance electrocatalytic processes and probably reduce the impacts of mass-transfer limitations [41]. Prior studies have also shown that Fe_2O_3 can enhance the electrochemical performance for OER by causing a synergistic impact between the two components and accelerating the inner transfer of electrons process inside the composite structure [42,43].

In order to create novel multifunctional composites and hybrids, it has been shown that it is beneficial to fabricate MOFs and effective materials. The derived hybrid material exhibit novel characteristics that have been shown to be favourable to those found in individual components obtained through the mutual beneficial linkage of the functional elements [44,45]. A structure of interconnected CNTs with integrated Co nanoparticles is made using ZIF-67 particles by Lou et al. It is reported that in situ generated MOF-based carbon nanotubes can significantly boost the electron transport [46]. The conductance of the MOF is improved by the extra nanoparticles, which enhances electrocatalysis for OER. Choi, Jonghyun, and coworkers effectively produced MOF-Co_3O_4 with a nanoflower-like structure and developed it on nickel foam [47], which acted as a conductive nanomaterial, using simple solvothermal and hydrothermal procedures. MOF-Co_3O_4 has an overpotential of 375 mV and 213 mV, according to oxygen evolution reaction (OER) and hydrogen evolution reaction (HER) [48].

Due to distinctive properties of MOFs, water electrolysis over Pr-MOFs-based electrode nanomaterials has a promising future because of its substantial binding sites, varied pore volume, size, three-dimensional structure, and rich coordinating chemistry [49,50]. According to this, MOF active regions can be created by combining different active linkers and metal components to synthesize the framework of the material. This can display an extremely remarkable synergistic effect, leading to considerably increased electrocatalytic performance.

On the other hand, rare elements have a common valence state of +3 and are easy to mix into stable compounds. The RE^{3+} ions have a variety of various electronic energy levels and eventually fill up their 4f orbitals. The filled 5s and 5p orbits act as a shield, reducing the sensitivity of the empty 4f orbits to their chemical environment, producing clearly defined electronic energy levels. Due to their unique structure and variety in oxidation states, materials based on rare earth elements show remarkable characteristics in a number of fields, such as luminescence, magnetic materials, catalysis, and energy conversion. As a result, we chose the Pr-MOF as compared to the transition metal-based MOF's. In addition to the strong interaction and rapid nucleation of Praseodymium ions and aromatic-based organic linkers the highly regulated direct synthesis of conductive Pr-MOF with efficient hollow nanostructures is still very challenging, and the synthesis of ion-confined conductive Pr-MOF based empty nanostructures as a promising oxygen electrocatalyst has only rarely been studied.

From the above motivated concerns, the choice of Pr-MOF with Fe_2O_3 nanocomposite for the oxygen evolution reaction (OER) was done on the basis of the specific structure and composition of the MOF. In this case, the Praseodymium can potentially be served as a catalytically active metal center within the MOF and may facilitating the transfer of electrons and promoting the desired chemical reactions to enhance the OER. Additionally, the presence of Pr can introduce specific redox properties, allowing for efficient electron transfer during the OER, and also can contribute to the stability of the MOF structure. Furthermore, the coordination of Pr with organic linkers can enhance the overall framework stability, preventing structural degradation during the OER. Hence, the combination of MOF with Fe_2O_3 can result in synergistic effects, enhancing the catalytic performance of the overall material. This can lead to improved OER activity, selectivity, and durability.

The hydrothermal process used in this project was to synthesize a novel nanocomposite of Pr-based MOF with Fe_2O_3 that utilise 1,3,5-benzenetricarboxylic acid as an organic ligand, which then demonstrated its electrocatalytic activities in 1 M potassium hydroxide as an electrolyte. Fe_2O_3 nanoparticles were believed to have a considerable effect on OER performance since they were introduced into the Pr-MOF's large porous framework. The Pr-MOF/Fe_2O_3 composite demonstrated a perfect Tafel plot of 39 mV dec^{-1}, indicating easy and rapid electron transmission throughout the OER response, and it achieved the standard power density of 10 mA cm^{-2} at just 238 mV. All of these parameters supported that the Pr-MOF/Fe2O3 nanocomposite has superior efficiency as

compared to single Pr-MOF and Fe_2O_3.

2. Experimental

2.1. Chemical reactant

All reagents with a known amount that were used as such i.e. copper nitrate ($Cu(NO_3)_2{\cdot}3H_2O$ (Analar, 99.8%)), N–N-Dimethlyformamide (DMF, Riedel-deHaen, 99%), acetone (Sigma adlrich, 99%), 1,3,5-benzenetricarboxylic acid (BTC, Sigma Aldrich, 99%), praseodymium (III) nitrate hexahydrate ($Pr(NO_3)_3{\cdot}6H_2O$ (Sigma Aldrich 98%), Iron nitrate ($Fe(NO_3)_3$, (Analar, 99.9%) and ethanol (Analar, 99.8%).

2.2. Formation of Fe_2O_3 nanoparticles

The solgel auto-combustion process was used to produce Fe_2O_3 nanoparticles. The $Fe(NO_3)_3{\cdot}9H_2O$ (0.05 M) precursor was mixed in 100 mL of distilled H_2O with 0.2 M citric acid solution. The pH of the solution was adjusted to 7–8 by pouring 2 M solvent of ammonia. Stirring the solution on a magnetic hotplate helps to distribute the components evenly and prevent the formation of clumps. This can result in a homogenous gel with consistent properties. The gel was burned between 200 and 250 °C to create the particles of brown color. Fe_2O_3 nanoparticles were produced by calcining the resulting ash at 550 °C for 5 h in a furnace.

2.3. Formation of Pr-MOF

N, N-dimethylformamide (DMF) (20 mL) was added to a reactor vessel to synthesize Pr-MOF. This solution was mixed with the specified amount of 1,3,5-benzenetricarboxylic acid (BTC, 0.212 g) while being stirred constantly to produce a homogenous solution. The above homogenous solution was continuously mixed for 10 min, then 0.221 g of $Pr(NO_3)_3{\cdot}6H_2O$ was also mixed. Stirring a mixture for 15 min is a common technique used to ensure that all the components are thoroughly mixed and react evenly. Transferring the mixture into a kept inside a stainless steel autoclave it at 160 °C temperature for 48 h. Finally, cooling the mixture back down to ambient temperature after a specified period of time. The MOF solution was additionally rinsed with ethanol, as well as some DMF was added during centrifugal filtration. Letting the material dry at room temperature overnight allows any residual solvent to evaporate and leaves behind the solid MOFs. Storing the dried MOFs in sample vials ensures that they will be protected from environmental factors that may cause degradation or contamination.

2.4. Synthesis of Pr-MOF/Fe_2O_3 composite

Taking the same actions as described above for the preparation of Pr-MOF, we vigorously stirred 20 mL of NN-dimethylformamide (DMF) by adding 1,3,5-benzenetricarboxylicacid (BTC, 0.21 g) which result into a transparent solution. At this stage, we continuously stirred the reaction mixture while adding nanoparticles Fe_2O_3 (0.1 g) and $Pr(NO_3)_3{\cdot}6H_2O$ (0.200 g). The rest of the processes were identical to those we used for the creation of Pr- MOF. In an autoclave lined with Teflon, the resultant mixture was heated to 160 °C for 48 h. The final composite material was obtained after rinsing with H_2O and ethanol during centrifugation and placed in an oven for drying where they were allowed to dry for 5 h at 60 °C and finally kept in a vacuum desiccator for further use.

2.5. Synthesis of working electrode

Nickel foam (NF) was employed as a substrate to create the working electrode for the electrocatalytic analysis. First, the nickel foam was cut into pieces of 1 cm × 1 cm as directed and then the NF pieces were sonicated for 15.0 min in each of the following solutions before being loaded with the fabricated materials HCl, ethanol, deionized water, and acetone. Following that, the cleaned NF electrodes were maintained in an electric oven set to 60.0 °C for drying. A homogeneous electrocatalyst slurry was formed by adding 5.0 mg of electrode material powder with 1.0 mL of DI water and ultrasonically processing it for an hour in order to examine the efficiency of the nanomaterials. The drop caste method was used to deposit Pr-MOF, Fe_2O_3 and Pr-MOF/Fe_2O_3 on NF pieces, which were subsequently dried for OER testing at ambient temperature.

2.6. Physical characterization

To acquire the diffractogram and examine crystal structure, orientation, and phase, an advanced Bruker D8 powder XRD equipment with Cu–K-alpha radiations was employed. Using Fourier-transform infrared spectroscopy (FTIR), it was shown how the atoms work together to generate functional groups that are responsible for the molecule's overall properties. A Bruker Tensor-27 with a 400–4000 cm^{-1} resolution was used for this purpose. Measurements using the scanning electron microscope (SEM, Nova Nano-SEM-450) were made to determine the particle size and shape. The NOVA2200e was employed to calculate the BET surface area, particle diameter, and pore volumes of the prepared nanocomposite materials using N_2 sorption isotherms.

2.7. Electrochemical characterization

By employing an AUTOLAB PGSTAT-204 electrocatalytic workstation in 1.0 M potassium hydroxide solution, the standard 3 electrode setup, which included a pt wire as a counter electrode, an Ag/AgCl standard electrode, and a coating of electrode materials on nickel foam (NF) as working electrode various techniques were employed. Cyclic voltammetry (CV), linear sweep voltammetry (LSV), electrochemical impedance spectroscopy (EIS) and electrochemical surface area (ECSA) techniques used to describe the electrochemical characteristics of nanoparticles for the OER and to understand how the materials can be optimized for this important energy conversion reaction. The given equation describes how to convert an Ag/AgCl (saturated KCl) standard electrode to RHE. The following equation (1) describes how to convert an Ag/AgCl (saturated potassium chloride) standard electrode to RHE (1).

$$ERHE = EAg/AgCl + 0.059\text{pH} + Eo\text{Ag/AgCl} \tag{1}$$

The overpotential value was calculated using equation (2):

$$\eta = E \text{ vs RHE} - 1.23\text{V} \tag{2}$$

The linear area of the polarisation curve was used to determine the Tafel plot for the electrocatalytic dynamics study, and overpotential was determined using equation (3).

$$\eta = \text{a} + \frac{2.303\text{RT}}{\alpha\text{nF}}\log j \tag{3}$$

A range of windows could be used from 0.90 to 1.20 V and various scanning ranges of 10, 20, and 30 mV s^{-1} in non-faradic locations, the double layer capacitance (*Cdl)* values were measured using ECSA using Equations (4) and (5) and the value of specific capacitance (*Cs*) was taken from the previously reported results [51].

$$Cdl = \frac{\text{Slope}}{2} \tag{4}$$

$$\text{ECSA} = \frac{Cdl}{Cs} \tag{5}$$

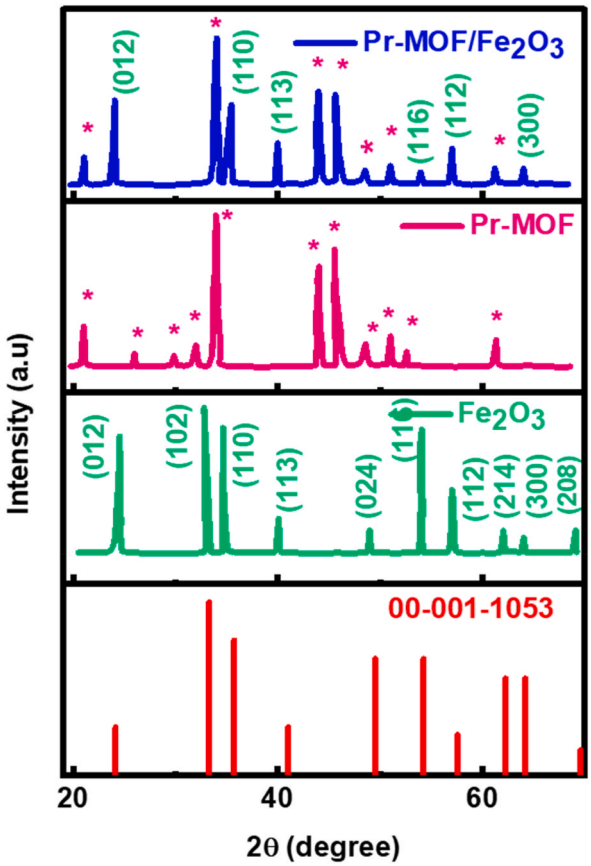

Fig. 1. XRD pattern of all synthesized materials.

During the electrochemical impedance spectroscopy (EIS) measurement, a voltage of 1.50 V was applied relative within a frequency range of 0.01–100 kHz to obtain the impedance spectrum of the system under investigation. Lower resistance to charge transfer is present in the semicircle in the low frequency zone and substantial electrical properties for the effective OER activity. The OER electrocatalyst's stability is a significant factor when employing it, and it may be assessed using CV and chronoamperometry at a fixed potential.

3. Results and discussion

3.1. Structural and morphological analysis

The XRD results of Fe_2O_3, Pr-MOF, and Pr-MOF/Fe_2O_3 nanocomposites were obtained using a X-ray diffractometer. Fig. 1 illustrates that the peaks of Fe_2O_3 with rhombohedral nanostructure at 2θ of 25°, 31°, 33°, 40°, 43°, 53°, 58°, 62°, 65°, and 68° that are also compatible with (JCPDS 00-001-1053). According to the strong and sharp peaks, the Fe_2O_3 nanostructures can be considered as crystalline in nature. Conversely, the existence of peaks at 2θ values of 21°, 27°, 28°, 31°, 33°, 43°, 46°, 49°, 52°, and 62° confirm that the Pr-MOF was polycrystalline in nature and that it had been prepared successfully. However, the Pr-MOF/Fe_2O_3 nanomaterial has

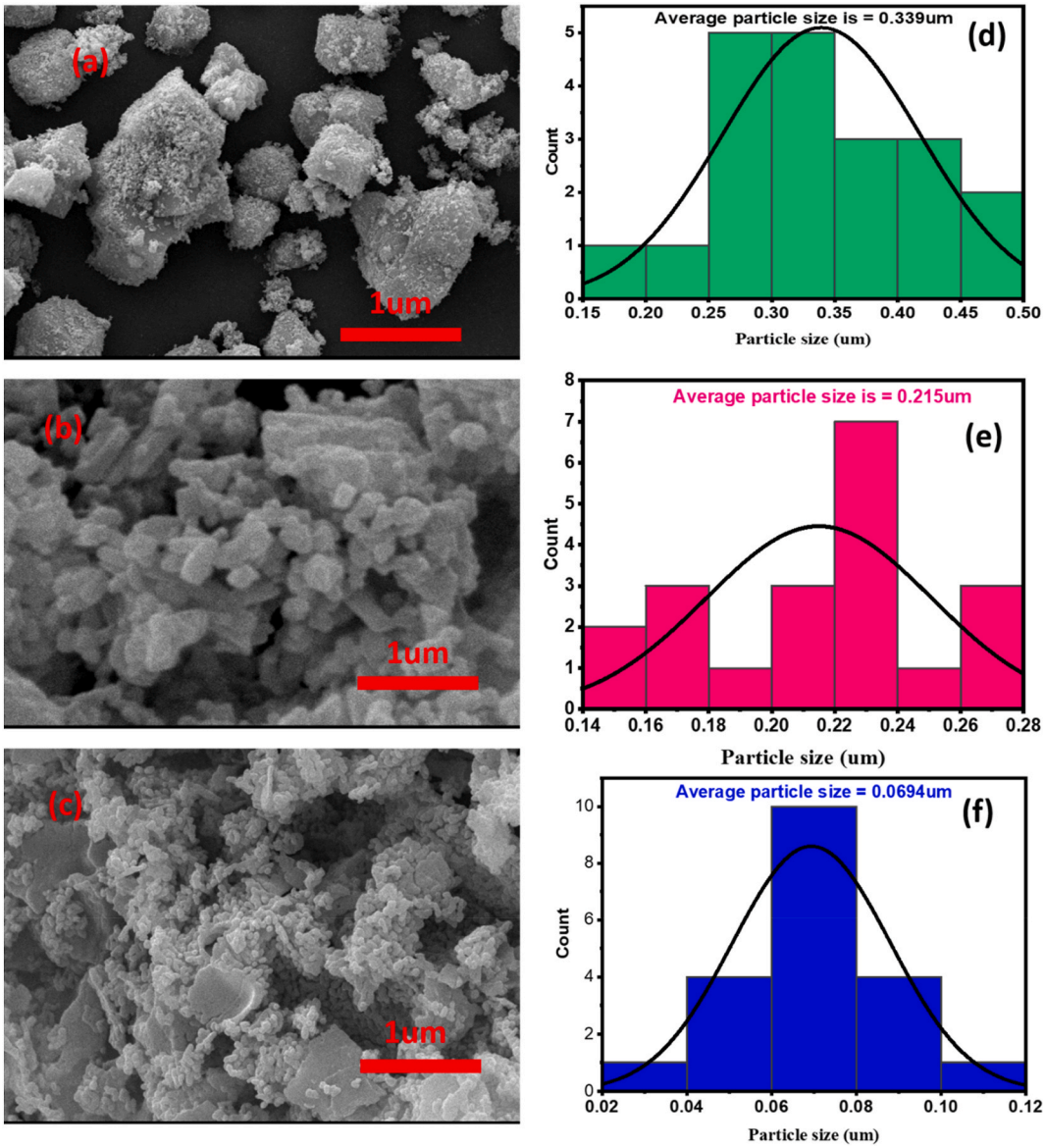

Fig. 2. (a) SEM micrograph of Fe_2O_3, (b) SEM micrograph of Pr-MOF, (c) SEM micrograph of Pr-MOF/Fe_2O_3, (d–f) Histogram of all synthesized materials.

been successfully synthesized as evidenced by the emergence of 7 peaks of Pr-MOF and 6 peaks of Fe_2O_3 in the Pr-MOF/Fe_2O_3 XRD spectrum, confirming both nanomaterials are present in the composite and the composite has been prepared successfully.

Fig. 2a displays SEM picture of Fe_2O_3, that demonstrates that microscopic nanoparticles are aggregated which is owing to their magnetic nature. The tiny disc-shaped morphology of the Pr-MOF was depicted in Fig. 2 (b). As shown in Fig. 2c, the interface of the tiny discs of Pr-MOF are adorned with magnetic particles. Here, also, the iron oxide particles are magnetically attracted to one another. A second indication that the nanocomposite had been efficiently formed was the presence of both materials' morphologies. The mean particle dimensions of the Fe_2O_3, Pr-MOF, and Pr-MOF/Fe_2O_3 composites are 0.399 μm, 0.215 μm, and 0.00694 μm, respectively, as shown in Fig. 2(d–f).

The FTIR pattern of Fe_2O_3 is shown in Fig. 3. In this case, the vibrational modes of the Fe–O bonds in the bending mode usually have bands at 496 and 659 cm^{-1} which confirm its successful formation. The bands at approximately 1669 and 3500 cm^{-1} are caused by hydroxyl ion bending and stretching vibrations caused by the deposition of H_2O on the interface of the nanomaterial [52,53]. The Pr-MOF and its composites functional groups are also shown in Fig. 3. This reveals that the molecules of H_2O in Pr-MOF are chemically linked during the dispersion of the solvent were responsible for the stronger band from 3452 cm^{-1}, which was brought on by the vibrational stretching of hydroxyl group. There are noticeable bands between the wavelengths of 1358 cm^{-1}, which are caused by the symmetrical vibrational stretching of the carbonate ions, and 1536 cm^{-1}, which is related to the asymmetric stretching of the carbonate ions [54]. The peak at 734 cm^{-1} illustrates the Pr–O stretching vibration. The presence of a distinct Pr-MOF spectrum in Pr-MOF/Fe_2O_3, as well as the loss of other distinct Fe_2O_3 bands and one separate Fe_2O_3 peak at 469 cm^{-1}, indicate that Pr^{3+} ions may have linked with the Fe_2O_3 nanoparticles. The Pr-MOF/Fe_2O_3 nanocomposite's open metal centers are linked by the oxygen in the Fe_2O_3 interface, possibly due to the disappearance of these bands for Fe_2O_3.

The N_2 adsorption-desorption isotherms demonstrated that a hierarchical permeability with a higher binding site for all synthesized materials was suggested by the pore size dispersion as shown in Fig. 4. The calculated BET active area of Fe_2O_3 was 68 m^2/g, for pure Pr-MOF was 420 m^2/g, and for Pr-MOF/Fe_2O_3 nanocomposite was 467.2 m^2/g. The findings suggest that Fe_2O_3 nanoparticles may have adhered to the Pr-MOF, enhancing its surface area and obstructing the pathways of the Pr-MOF. The hybrid material's greater surface area implies that it has greater binding sites accessible for the reactive compound deposition on its interface, which is the first stage in OER process.

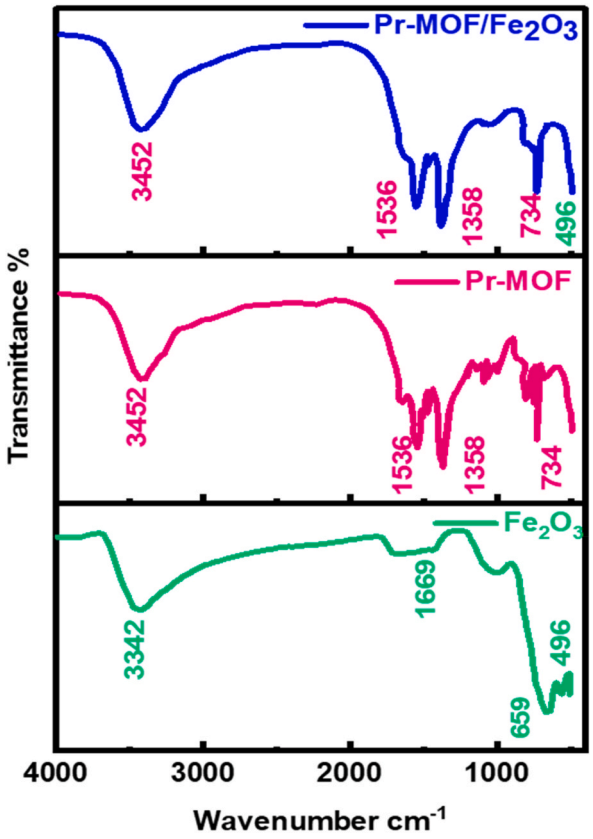

Fig. 3. FTIR analysis of all synthesized materials.

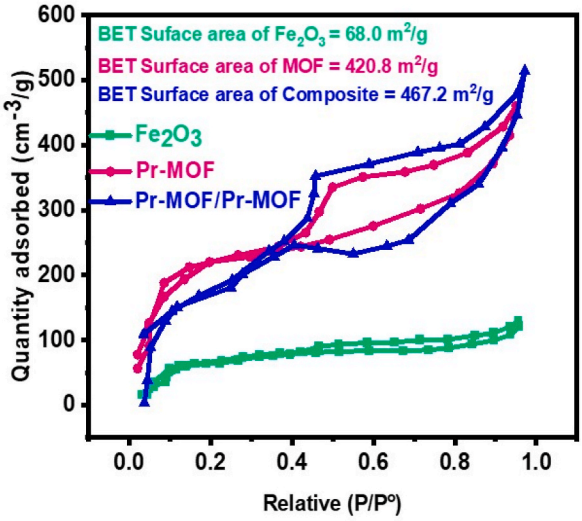

Fig. 4. BET isotherm of all synthesized materials.

3.2. *Electrocatalytic measurements*

It was feasible to evaluate the electrocatalytic properties of synthesized materials for the water splitting using CV and LSV. The polarisation curves for the nanomaterials deposited on the NF in aqueous solution (1 M Potassium hydroxide) are illustrated in Fig. 5 (a–c). For Fe_2O_3, Pr-MOF and Pr-MOF/Fe_2O_3, the onset potential were found to be 1.60, 1.54, and 1.41 V vs. RHE, respectively. These

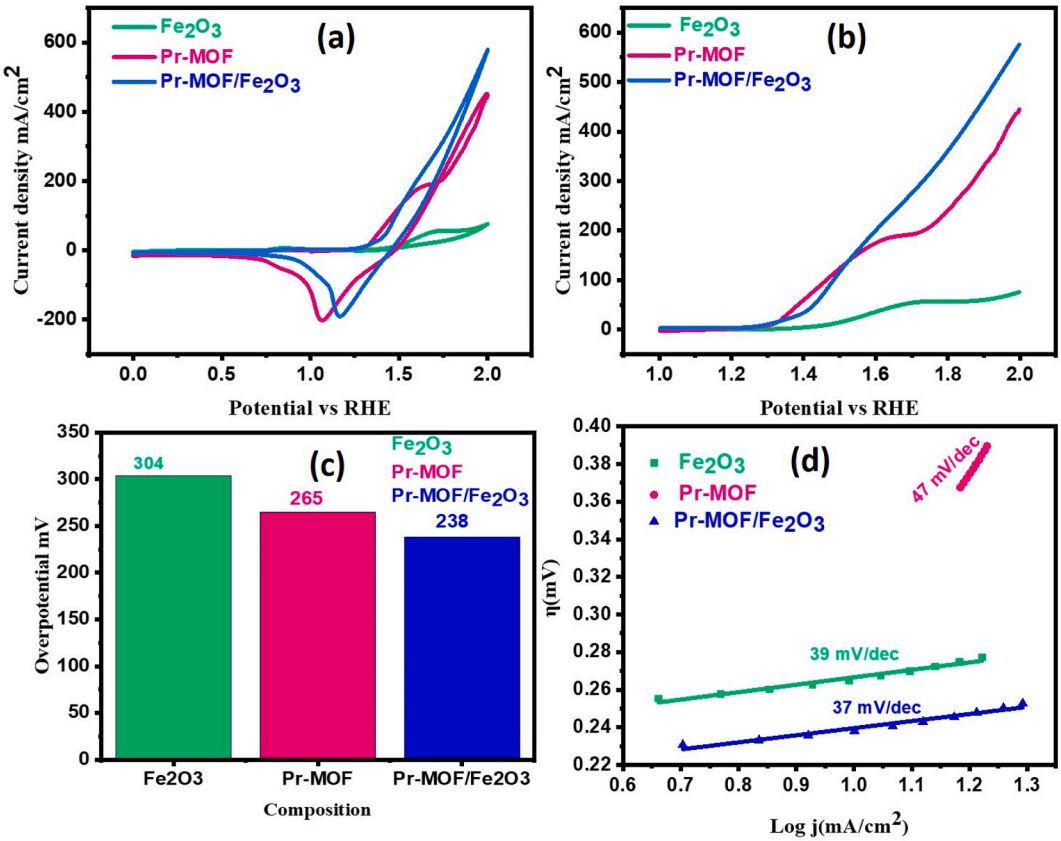

Fig. 5. (a) Cyclic voltammogram, (b) Linear sweep voltammogram, (c) Overpotentials Comparison at 10 mA cm^{-2} current density (d) Tafel slope of Fe_2O_3, Pr-MOF and Pr-MOF/Fe_2O_3.

results demonstrated the exceptional propensity of the as-synthesized Pr-MOF nanocomposite to start the OER at an extremely low onset potential. Any electrocatalyst used during OER can have inherent potential, but typically a current density in the region of 10 mA cm^{-2} is considered as the starting point. The overpotential values for Pr-MOF/Fe_2O_3, Pr-MOF and Fe_2O_3 were 238, 265, and 304 mV, correspondingly, when observed at 10 mA cm^{-2}.

The obtained overpotential values demonstrated that even with a somewhat low onset potential, the Pr-MOF/Fe_2O_3 showed superior OER performance than pure Fe_2O_3 and Pr-MOF. Because Fe_2O_3 nanoparticles promote Pr-MOF/Fe_2O_3, which has smaller overpotential than Pr-MOF and Fe_2O_3, it has the best catalytic performance towards OER in aqueous environment. This will lead to an improvement in the electrochemical performance towards OER of Pr-MOF/Fe_2O_3 owing to the electronic instability and the rise of binding sites of Pr-MOF/Fe_2O_3 nanocomposites. Moreover, a large rise in electrical conductivity and electrocatalytic active region, as well as the synergistic impact among Fe_2O_3 and Pr-MOF on the heterojunction interface and the active particles of Fe_2O_3 formed in situ, result in improved electrocatalytic performance. As a catalyst for splitting water, MOF-based nanocomposites (Pr-MOF/Fe_2O_3) perform significantly as compare to Pr-MOF and Fe_2O_3 because they easily collapse, fuse, and aggregate at high temperatures, reducing the mass transfer capability and availability of the catalyst's active regions. The total amount of active sites and the electrocatalytic performance should both be increased, Fe_2O_3 nanoparticles are hybridized. In comparison to Fe_2O_3, Pr-MOF, and physical mixture, the (Pr-MOF/Fe_2O_3) composite exhibits superior OER activity due to Pr-MOF's larger permeability and active surface region, Fe_2O_3 nanoparticles enhanced redox capacity, and its combined impact.

The increased electrocatalytic performance Pr-MOF/Fe_2O_3 is most likely as a result of extra open surface active catalytic regions. The value of the Tafel slope was determined using a linear equation, taking into account the linear portion of the steady-state polarisation graph. Lower values of Tafel slope are associated with simple adsorption/desorption via fast transfer of charges across the catalyst's surface, which confers enhanced activity to it. Higher values are associated with the catalyst behaving in a highly resistive manner during transfer of charge, which results in small adsorption/desorption, which confers unfavorable electrocatalytic characters to the electrocatalyst. The porous nature of the suggested material also enhanced electron transport. By determining the polarisation loops that related to each electrode material, as can be shown in Fig. 5 (d), Tafel plots of the different electrode materials are produced. The Tafel plot of Pr-MOF/Fe_2O_3 is significantly less (37 mV dec^{-1}) than that of Fe_2O_3 (39 mV dec^{-1}) and Pr-MOF (47 mV dec^{-1}), indicating fast OER dynamics. One of the polarisation curves, the Tafel plot, is situated in a strongly polarised region. A lower value of the Tafel slope is projected to result in higher voltage and lower electrode resistance during polarisation. Due to the material's high surface area, porosity, and quantity of visible active regions for the desorption and adsorption of reaction intermediates, Pr-MOF/Fe_2O_3 is an excellent electrode material for enhancing OER with great potential. On the other hand, at a scan rate of 30 mV s^{-1}, the overpotential has also been assessed using the cyclic voltammetry curves as shown in Fig. 6, and was used to investigate the intrinsic voltage of any OER electrode materials. The value of the resultant overpotential at 30 mV s^{-1} were 245 and 257 mV for Pr-MOF/Fe_2O_3 and Pr-MOF, respectively. The obtained overpotential values demonstrated that the composites materials showed superior OER performance than Pr-MOF. As the scan rate increases the overpotential also increases due to the less contact time between the electrode and electrolyte.

The synthesized Pr-MOF/Fe2O3 composites shown in 'M' contain active Pr active sites that can serve as an example of the general mechanism for OER. In equation (6), the oxidation of OH- ion in the initial stage, which led to the creation of M − OH, caused the accumulation of OH radicals on the interface of open active areas. In equation (7), it is shown that the coupled e-s and protons that are eliminated from the M − OH lead to the formation of M-O. However, when combined with 1 electron, Metal hydroperoxide (M-OOH), which is produced by a nucleophilic attack on the M-OOH, is obtained from equation (8). In equation (9), an open catalytic surface is produced and an O2 molecule is released as a result of the proton's contact with an extra electron.

$$M^{*}+ OH^{-} \rightarrow M^{*}OH + e^{-} \quad (6)$$

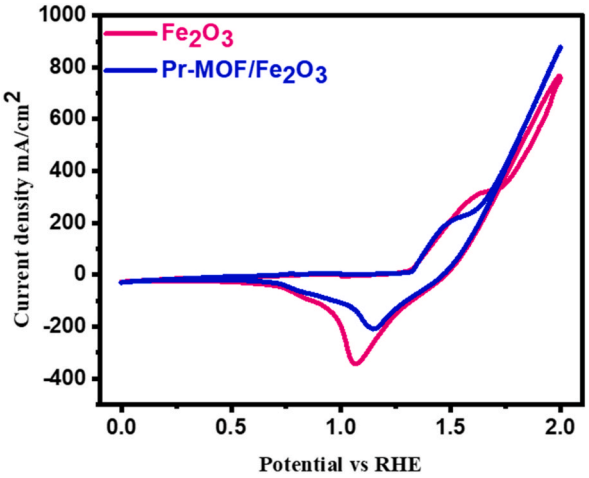

Fig. 6. Cyclic voltammogram of Pr-MOF/Fe_2O_3 and Pr-MOF at 30 mV s^{-1}.

$$M^*OH + OH^- \rightarrow M^*O + H2O + e^- \quad (7)$$

$$M^*O + OH^- \rightarrow M^*OOH + e^- \quad (8)$$

$$M^*OOH + OH^- \rightarrow M^*O2 + H2O + e^- \quad (9)$$

The conductivity of the appropriate electrochemical solution in addition to any electrocatalysts were also estimated using impedance measurements. When compared to pure Fe_2O_3 and Pr-MOF, the electrocatalyst Pr-MOF/Fe_2O_3, the Nyquist plots depict a smaller semicircle, as seen in Fig. 7. This shows the strong electrocatalytic activity of the nanocomposites, which supports the charge transfer reaction during electrocatalytic water electrolysis Furthermore, homogeneous Fe_2O_3 dispersion on MOFs and strong adhesion between the MOF framework and the Fe_2O_3 support lead to exposed active sites, easy and rapid transfer of electrons, and efficient coordination among two metals, which advantageously contributes to mechanical strengthening, rapid dynamics, and improved electric transmission of electrochemical materials by reducing resistance.

ECSA only displays the actual quantity of catalyst needed to finish the slow OER. The number of open active areas will increase together with the ECSA value, greatly enhancing the electrocatalyst's performance. In a non-Faradic zone, multiple CV plots were collected at varied sweep rates of 10, 20, and 30 mV s^{-1} as shown in Fig. 8(a–c). The difference in power density (j) among the anode and the cathode was calculated using the data from these graphs to obtain the j values. The straight-line curve produced by plotting the values of j against the above mentioned scan rate revealed that the double-layer capacitance (Cdl) values for Fe_2O_3, Pr-MOF and Pr-MOF/Fe_2O_3 are, respectively, 1.05 mF, 7.05 mF, and 9.5 mF as shown in Fig. 8(d–f). In order to calculate the ECSA value, the Cdl value was multiplied by the specific capacitance (0.040 mF cm^{-2}) and the result was found to be 26.25, 176, 237 cm^2 for Fe_2O_3, Pr-MOF and Pr-MOF/Fe_2O_3. Because Pr-MOF/Fe_2O_3 composite exhibited higher ECSA values, there was no doubt that these materials contained a lot of active sites, and that these sites were exposed to and actively involved in the electron-proton transition at electrolyte-electrode contacts during electrolysis. The composite's impressive catalytic activity and higher value of ECSA were further assisted by its increased BET surface area (467.2 m^2/g), which allowed for maximum exposure of electrochemical active regions.

The produced nanocomposite Pr-MOF/Fe_2O_3 exhibits outstanding OER activity that is equivalent to or superior to that of metal oxide and MOF based OER electrocatalysts, as shown in Table 1. This is based on the measurements mentioned above. An electrode material must be stable enough for practical use even at high activity levels. The synthesized nanocomposite increased electrocatalytic activity and stayed stable in experiments including 2000 CV cycles in 1.0 M KOH solution at 50 mV s^{-1}. Fig. 9a shows a small difference between the 1st and 2000th cycles in CV cycles. As seen in Fig. 9 (b), chronoamperometry was used to assess the electrolytic stability for 40 h at 0.8 V vs. an Ag/AgCl electrode in a 1.0 M alkaline solution. Activity remained essentially constant during electrolysis, with a slight drop with time, according to time-versus-current density graphs. The XRD data revealed that although the peak position in the XRD spectrum of the nanocomposites (Fig. 9c) remained unchanged, the peak intensity had barely changed, demonstrating that the nanocomposite's structure is robust. According to the findings of XRD, Chronoamperometry, and CV, the nanomaterial is highly stable.

4. Summary

The development of rare earth metal based MOF nanocomposites (Pr-MOF) catalysts using transition metal oxides (Fe_2O_3) offers hope for the efficient OER. Under controlled conditions, hydrothermal synthesis method was used for the production of the innovative composite material Pr-MOF/Fe_2O_3 successfully. The successful synthesis of the necessary phases in the nanocomposite material was confirmed by XRD and FTIR, while SEM indicated good morphology and BET illustrated specific surface area. The Pr-MOF/Fe_2O_3

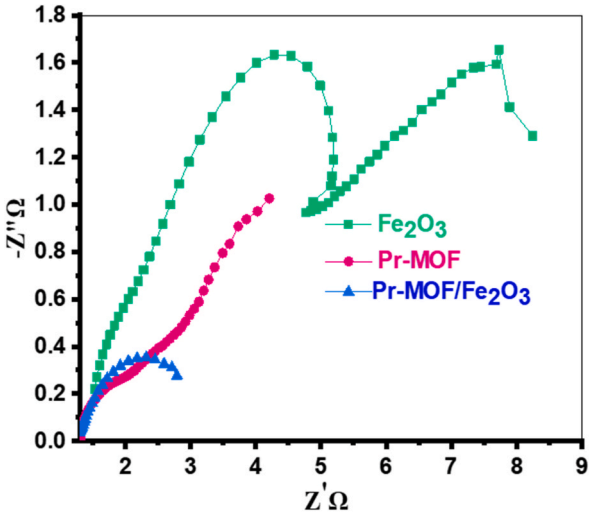

Fig. 7. EIS studies of Fe_2O_3, Pr-MOF and Pr-MOF/Fe_2O_3.

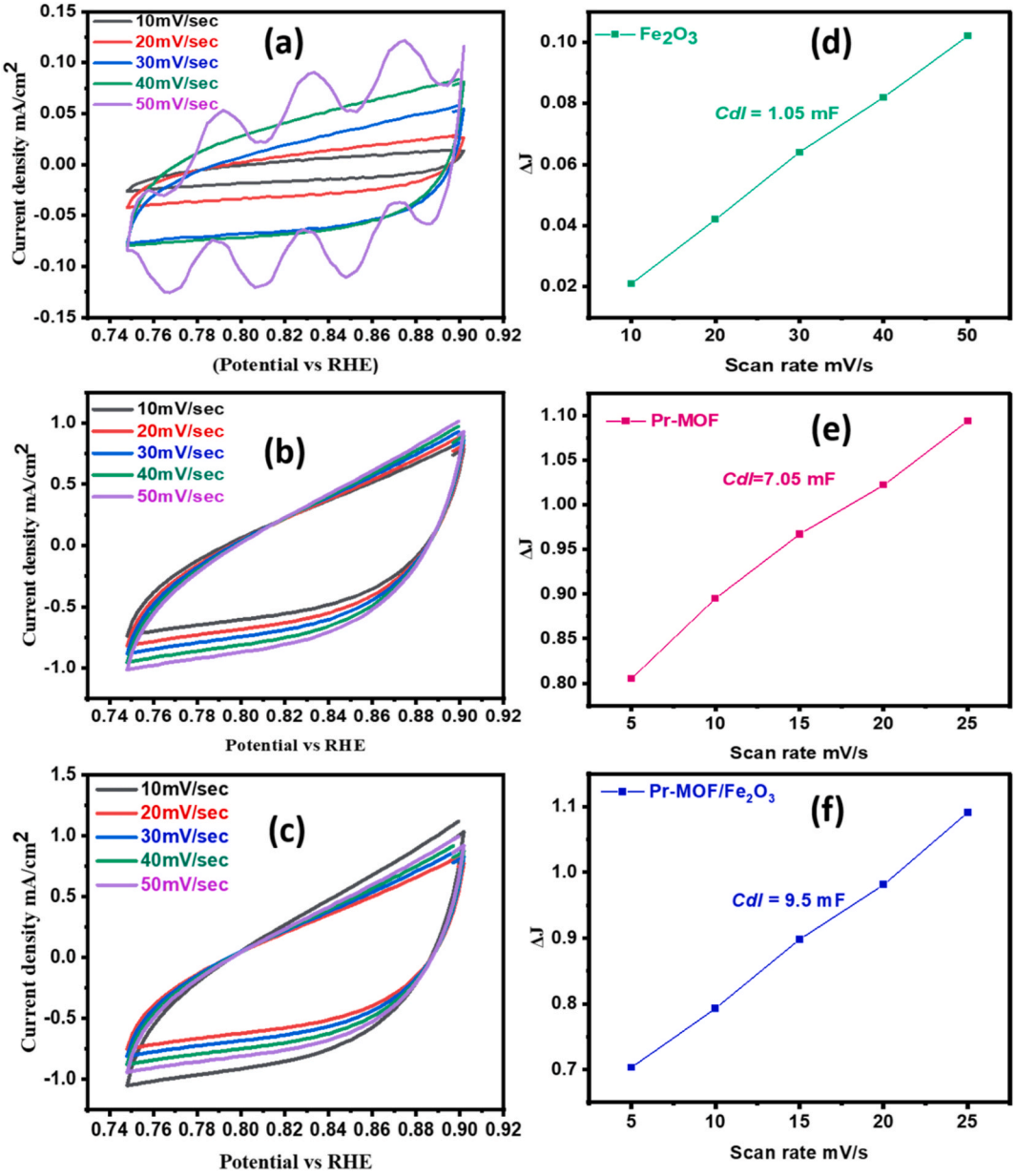

Fig. 8. (a–c) ECSA plots (d–f) Corresponding Cdl curves for all synthesized materials.

nanocomposite exhibited remarkable OER at 10 mA cm^{-2} with a low onset potential (1.41 V), overpotential (238 mV), and a reduced Tafel slope value of 37 mV dec^{-1}. The composite materials showed good long-term stability with no change in current density or decline in performance in 1 M alkaline solution (KOH). This places the electrocatalyst at the forefront of water electrolysis technology for effective OER and overall hydrogen fuel synthesis.

Author contribution statement

Bushra Shabbir: Sumaira Manzoor: Conceived and designed the experiments; Performed the experiments; Wrote the paper. Karam Jabbour: Khaled Fahmi Fawy: Contributed reagents, materials, analysis tools or data. Muhammad Faheem Ashiq: Performed the experiments; Wrote the paper. Muhammad Ashiq: Analyzed and interpreted the data.

Data availability statement

Data will be made available on request.

Table 1
The OER activity of several MOFs and their nanocomposites electrochemically.

Ser.No	Electrocatalyst	Electrolyte	Substrate	Overpotential mV	Tafel slope mV/dec	References
1	CoFe 2D MOF	KOH	GC	274	46	[55]
2	Ni-MOF@Fe-MOF	KOH	GC	265	83	[56]
3	MIL-53(CoeFe	KOH	NF	262	69	[57]
4	Ni0·5Co0.5-MOF-74	KOH	GC	270	49	[58]
5	Co_3S_4/EC-MOF	KOH	CC	236	122	[59]
6	Ni-BDC@NiS	KOH	NF	330	62	[60]
7	CoS_x/Co-MOF	KOH	NF	280	83	[61]
8	Co_3O_4@Co-MO	KOH	GC	277	79	[62]
9	$Co(OH)_2$/Co-MOF	KOH	GC	225	107	[63]
10	$Fe(OH)_3$@Co-MOF-74	KOH	CP	292	44	[64]
11	NiCo-UMOFNs	KOH	GC	260	32	[65]
12	Co-MONs	KOH	GC	309	75.5	[65]
13	**Pr-MOF/Fe_2O_3**	**KOH**	**NF**	**238**	**37**	**Present work**

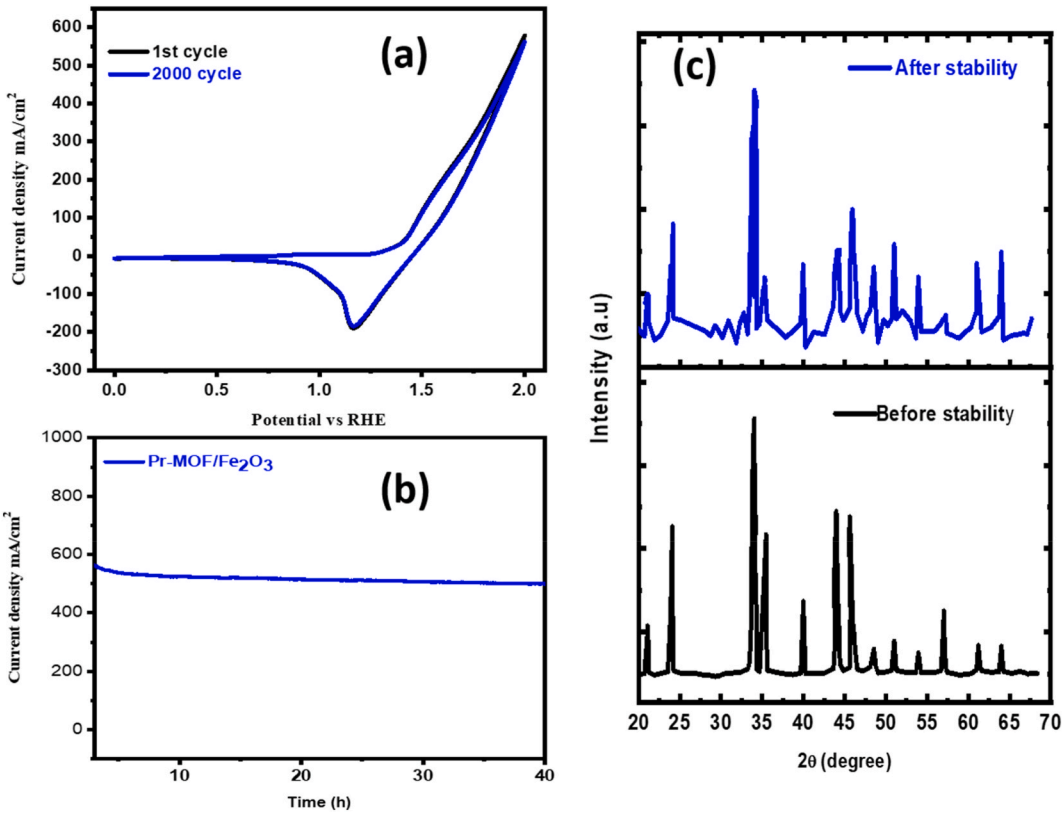

Fig. 9. (a) CV cycles (b) Chronoamperometry of Pr-MOF/Fe_2O_3 (c) XRD pattern of Pr-MOF/Fe_2O_3 before and after stability.

Declaration of competing interest

The authors declare that they have no known competing financial interests or personal relationships that could have appeared to influence the work reported in this paper.

The manuscript has not been published previously, and is not under consideration for publication elsewhere. It is also stated that the work is original. The publication is approved by all authors and tacitly or explicitly by the responsible authorities where the work was carried out. If accepted, it will not be published elsewhere in the same form, in English or in any other language, including electronically without the written consent of the copyright-holder. In addition, the authors have no conflicts of interest to declare.

Acknowledgements

M. N. Ashiq is thankful to Bahauddin Zakariya University, Multan, Pakistan for providing financial assistance (ORIC/2023/155). K.

F.F express appreciation to the Deanship of Scientific Research at King Khalid University Saudi Arabia for funding through research groups program under grant number R.G.P. 2/279/44.

References

[1] A. Coradini, F. Capaccioni, P. Drossart, G. Arnold, E. Ammannito, F. Angrilli, G. Tozzi, VIRTIS: an imaging spectrometer for the Rosetta mission, Space Sci. Rev. 128 (2007) 529–559.
[2] J.P. Dorian, H.T. Franssen, D.R. Simbeck, Global challenges in energy, Energy Pol. 34 (15) (2006) 1984–1991.
[3] J.R. Riba, C. López-Torres, L. Romeral, A. Garcia, Rare-earth-free propulsion motors for electric vehicles: a technology review, Renew. Sustain. Energy Rev. 57 (2016) 367–379.
[4] B. Schlamadinger, M. Apps, F. Bohlin, L. Gustavsson, G. Jungmeier, G. Marland, I. Savolainen, Towards a standard methodology for greenhouse gas balances of bioenergy systems in comparison with fossil energy systems, Biomass Bioenergy 13 (6) (1997) 359–375.
[5] B.E. Rittmann, Opportunities for renewable bioenergy using microorganisms, Biotechnol. Bioeng. 100 (2) (2008) 203–212.
[6] A. Gasparatos, C.N. Doll, M. Esteban, A. Ahmed, T.A. Olang, Renewable energy and biodiversity: implications for transitioning to a green economy, Renew. Sustain. Energy Rev. 70 (2017) 161–184.
[7] L. Barreto, A. Makihira, K. Riahi, The hydrogen economy in the 21st century: a sustainable development scenario, Int. J. Hydrogen Energy 28 (3) (2003) 267–284.
[8] K. Mazloomi, C. Gomes, Hydrogen as an energy carrier: prospects and challenges, Renew. Sustain. Energy Rev. 16 (5) (2012) 3024–3033.
[9] M. Karczewski, J. Chojnowski, G. Szamrej, A review of low-CO_2 emission fuels for a dual-fuel RCCI engine, Energies 14 (16) (2021) 5067.
[10] C. Zhang, Y. Yu, M.E. Grass, C. Dejoie, W. Ding, K. Gaskell, B.W. Eichhorn, Mechanistic studies of water electrolysis and hydrogen electro-oxidation on high temperature ceria-based solid oxide electrochemical cells, J. Am. Chem. Soc. 135 (31) (2013) 11572–11579.
[11] A. Aijaz, J. Masa, C. Rösler, W. Xia, P. Weide, A.J. Botz, M. Muhler, Co@ Co3O4 encapsulated in carbon nanotube-grafted nitrogen-doped carbon polyhedra as an advanced bifunctional oxygen electrode, Angew. Chem. Int. Ed. 55 (12) (2016) 4087–4091.
[12] J. Wang, F. Xu, H. Jin, Y. Chen, Y. Wang, Non-noble metal-based carbon composites in hydrogen evolution reaction: fundamentals to applications, Adv. Mater. 29 (14) (2017), 1605838.
[13] T. Asefa, X. Huang, Heteroatom-Doped carbon materials for electrocatalysis, Chem.–Eur. J. 23 (45) (2017) 10703–10713.
[14] Y. Yan, B.Y. Xia, B. Zhao, X. Wang, A review on noble-metal-free bifunctional heterogeneous catalysts for overall electrochemical water splitting, J. Mater. Chem. A 4 (45) (2016) 17587–17603.
[15] X. Zou, Y. Zhang, Noble metal-free hydrogen evolution catalysts for water splitting, Chem. Soc. Rev. 44 (15) (2015) 5148–5180.
[16] H. Lu, J. Tournet, K. Dastafkan, Y. Liu, Y.H. Ng, S.K. Karuturi, Z. Yin, Noble-metal-free multicomponent nanointegration for sustainable energy conversion, Chem. Rev. 121 (17) (2021) 10271–10366.
[17] C. Richard, B. Viana, Persistent X-ray-activated phosphors: mechanisms and applications, Light Sci. Appl. 11 (1) (2022) 123.
[18] Y. Sun, T. Zhang, C. Li, K. Xu, Y. Li, Compositional engineering of sulfides, phosphides, carbides, nitrides, oxides, and hydroxides for water splitting, J. Mater. Chem. A 8 (27) (2020) 13415–13436.
[19] B.R. Wygant, K. Kawashima, C.B. Mullins, Catalyst or precatalyst? The effect of oxidation on transition metal carbide, pnictide, and chalcogenide oxygen evolution catalysts, ACS Energy Lett. 3 (12) (2018) 2956–2966.
[20] S.J. Lee, J. Theerthagiri, P. Nithyadharseni, P. Arunachalam, D. Balaji, A.M. Kumar, M.Y. Choi, Heteroatom-doped graphene-based materials for sustainable energy applications: a review, Renew. Sustain. Energy Rev. 143 (2021), 110849.
[21] Y. Yu, S.J. Lee, J. Theerthagiri, Y. Lee, M.Y. Choi, Architecting the AuPt alloys for hydrazine oxidation as an anolyte in fuel cell: comparative analysis of hydrazine splitting and water splitting for energy-saving H2 generation, Appl. Catal. B Environ. 316 (2022), 121603.
[22] S.N. Shreyanka, J. Theerthagiri, S.J. Lee, Y. Yu, M.Y. Choi, Multiscale design of 3D metal–organic frameworks (M− BTC, M: Cu, Co, Ni) via PLAL enabling bifunctional electrocatalysts for robust overall water splitting, Chem. Eng. J. 446 (2022), 137045.
[23] Y. Yu, J. Theerthagiri, S.J. Lee, G. Muthusamy, M. Ashokkumar, M.Y. Choi, Integrated technique of pulsed laser irradiation and sonochemical processes for the production of highly surface-active NiPd spheres, Chem. Eng. J. 411 (2021), 128486.
[24] J. Theerthagiri, S.J. Lee, A.P. Murthy, J. Madhavan, M.Y. Choi, Fundamental aspects and recent advances in transition metal nitrides as electrocatalysts for hydrogen evolution reaction: a review, Curr. Opin. Solid State Mater. Sci. 24 (1) (2020), 100805.
[25] X. Xiao, L. Zou, H. Pang, Q. Xu, Synthesis of micro/nanoscaled metal–organic frameworks and their direct electrochemical applications, Chem. Soc. Rev. 49 (1) (2020) 301–331.
[26] S.S.A. Shah, T. Najam, M.K. Aslam, M. Ashfaq, M.M. Rahman, K. Wang, Y. Wang, Recent advances on oxygen reduction electrocatalysis: correlating the characteristic properties of metal organic frameworks and the derived nanomaterials, Appl. Catal. B Environ. 268 (2020), 118570.
[27] T. Wang, X. Cao, L. Jiao, Progress in hydrogen production coupled with electrochemical oxidation of small molecules, Angew. Chem. Int. Ed. 61 (51) (2022), e202213328.
[28] T. Wang, L. Miao, S. Zheng, H. Qin, X. Cao, L. Yang, L. Jiao, Interfacial engineering of Ni3N/Mo2N heterojunctions for urea-assisted hydrogen evolution reaction, ACS Catal. 13 (7) (2023) 4091–4100.
[29] X. Cao, C. Tan, M. Sindoro, H. Zhang, Hybrid micro-/nano-structures derived from metal–organic frameworks: preparation and applications in energy storage and conversion, Chem. Soc. Rev. 46 (10) (2017) 2660–2677.
[30] R.R. Salunkhe, Y.V. Kaneti, Y. Yamauchi, Metal–organic framework-derived nanoporous metal oxides toward supercapacitor applications: progress and prospects, ACS Nano 11 (6) (2017) 5293–5308.
[31] P. Lang, N. Yuan, Q. Jiang, Y. Zhang, J. Tang, Recent advances and prospects of metal-based catalysts for oxygen reduction reaction, Energy Technol. 8 (3) (2020), 1900984.
[32] N. Cheng, L. Ren, X. Xu, Y. Du, S.X. Dou, Recent development of zeolitic imidazolate frameworks (ZIFs) derived porous carbon based materials as electrocatalysts, Adv. Energy Mater. 8 (25) (2018), 1801257.
[33] E. Pervaiz, M. Ali, M.A. Abbasi, T. Noor, Z. Said, H. Alawadhi, Unfolding essence of nanoscience for improved water splitting hydrogen generation in the light of newly emergent nanocatalysts, Int. J. Hydrogen Energy 47 (63) (2022) 26915–26955.
[34] S.S.A. Shah, T. Najam, M. Wen, S.Q. Zang, A. Waseem, H.L. Jiang, Metal–organic framework-based electrocatalysts for CO_2 reduction, Small Structures 3 (5) (2022), 2100090.
[35] A. Mirzaei, B. Hashemi, K. Janghorban, α-Fe 2 O 3 based nanomaterials as gas sensors, J. Mater. Sci. Mater. Electron. 27 (2016) 3109–3144.
[36] S. Behrens, Preparation of functional magnetic nanocomposites and hybrid materials: recent progress and future directions, Nanoscale 3 (3) (2011) 877–892.
[37] Y. Guo, Q. Huang, J. Ding, L. Zhong, T.T. Li, J. Pan, S. Huang, CoMo carbide/nitride from bimetallic MOF precursors for enhanced OER performance, Int. J. Hydrogen Energy 46 (43) (2021) 22268–22276.
[38] D. Chen, Q. Sun, C. Han, Y. Guo, Q. Huang, W.A. Goddard, J. Qian, Enhanced oxygen evolution catalyzed by in situ formed Fe-doped Ni oxyhydroxides in carbon nanotubes, J. Mater. Chem. A 10 (30) (2022) 16007–16015.
[39] D. Mendes, A. Mendes, L.M. Madeira, A. Iulianelli, J.M. Sousa, A. Basile, The water-gas shift reaction: from conventional catalytic systems to Pd-based membrane reactors—a review, Asia Pac. J. Chem. Eng. 5 (1) (2010) 111–137.
[40] W.A. Qureshi, S.N.U.Z. Haider, A. Naveed, A. Ali, Q. Liu, J. Yang, Recent progress in the synthesis, characterization and photocatalytic application of energy conversion over single metal atoms decorated graphitic carbon nitride, Int. J. Hydrogen Energy (2023).
[41] S. Xu, Q. Huang, J. Xue, Y. Yang, L. Mao, S. Huang, J. Qian, Morphologically controlled metal–organic framework-derived FeNi oxides for efficient water oxidation, Inorg. Chem. 61 (23) (2022) 8909–8919.

[42] C. Ray, T. Pal, Retracted Article: recent advances of metal–metal oxide nanocomposites and their tailored nanostructures in numerous catalytic applications, J. Mater. Chem. A 5 (20) (2017) 9465–9487.
[43] J. Tang, C. Su, Z. Shao, Covalent organic framework (COF)-Based hybrids for electrocatalysis: recent advances and perspectives, Small Methods 5 (12) (2021), 2100945.
[44] J. Tang, C. Su, Z. Shao, Covalent organic framework (COF)-Based hybrids for electrocatalysis: recent advances and perspectives, Small Methods 5 (12) (2021), 2100945.
[45] M. Mahmoudpour, S. Ding, Z. Lyu, G. Ebrahimi, D. Du, J.E.N. Dolatabadi, Y. Lin, Aptamer functionalized nanomaterials for biomedical applications: recent advances and new Horizons, Nano Today 39 (2021), 101177.
[46] C. Wang, J. Kim, J. Tang, M. Kim, H. Lim, V. Malgras, Y. Yamauchi, New strategies for novel MOF-derived carbon materials based on nanoarchitectures, Chem 6 (1) (2020) 19–40.
[47] M.K. Lee, M. Shokouhimehr, S.Y. Kim, H. Jang, Two-dimensional metal–organic frameworks and covalent–organic frameworks for electrocatalysis: distinct merits by the reduced dimension, Adv. Energy Mater. 12 (2022), 2003990.
[48] L. Mollà Guerola, Aminación de dobles enlaces mediada por alcoholes fluorados, 2023.
[49] H. Wu, Q. Lu, Y. Li, M. Zhao, J. Wang, Y. Li, W. Hu, Structural framework-guided universal design of high-entropy compounds for efficient energy catalysis, J. Am. Chem. Soc. 145 (3) (2022) 1924–1935.
[50] J. Li, Y. Liu, H. Chen, Z. Zhang, X. Zou, Design of a multilayered oxygen-evolution electrode with high catalytic activity and corrosion resistance for saline water splitting, Adv. Funct. Mater. 31 (27) (2021), 2101820.
[51] P. Babar, A. Lokhande, V. Karade, B. Pawar, M.G. Gang, S. Pawar, J.H. Kim, Towards highly efficient and low-cost oxygen evolution reaction electrocatalysts: an effective method of electronic waste management by utilizing waste Cu cable wires, J. Colloid Interface Sci. 537 (2019) 43–49.
[52] M.M. Mohamed, E.E. Abdelmonem, G.O. El-Sayed, Graphene foam mediated FeS2/α-Fe2O3 composites for chloramphenicol photodegradation using persulfate activation under visible light irradiation, J. Water Proc. Eng. 53 (2023), 103633.
[53] P. Mishra, A. Behera, D. Kandi, S. Ratha, K. Parida, Novel magnetic retrievable visible-light-driven ternary Fe3O4@ NiFe2O4/phosphorus-doped g-C3N4 nanocomposite photocatalyst with significantly enhanced activity through a double-Z-scheme system, Inorg. Chem. 59 (7) (2020) 4255–4272.
[54] G. Lakshminarayana, S.O. Baki, A. Lira, I.V. Kityk, U. Caldiño, K.M. Kaky, M.A. Mahdi, Structural, thermal and optical investigations of Dy3+-doped B2O3–WO3–ZnO–Li2O–Na2O glasses for warm white light emitting applications, J. Lumin. 186 (2017) 283–300.
[55] L. Zhuang, L. Ge, H. Liu, Z. Jiang, Y. Jia, Z. Li, Z. Zhu, A surfactant-free and scalable general strategy for synthesizing ultrathin two-dimensional metal–organic framework nanosheets for the oxygen evolution reaction, Angew. Chem. 131 (38) (2019) 13699–13706.
[56] K. Rui, G. Zhao, Y. Chen, Y. Lin, Q. Zhou, J. Chen, S.X. Dou, Hybrid 2D dual-metal–organic frameworks for enhanced water oxidation catalysis, Adv. Funct. Mater. 28 (26) (2018), 1801554.
[57] M. Xie, Y. Ma, D. Lin, C. Xu, F. Xie, W. Zeng, Bimetal–organic framework MIL-53 (Co–Fe): an efficient and robust electrocatalyst for the oxygen evolution reaction, Nanoscale 12 (1) (2020) 67–71.
[58] J. Tian, F. Jiang, D. Yuan, L. Zhang, Q. Chen, M. Hong, Electric-field assisted in situ hydrolysis of bulk metal–organic frameworks (MOFs) into ultrathin metal oxyhydroxide nanosheets for efficient oxygen evolution, Angew. Chem. Int. Ed. 59 (31) (2020) 13101–13108.
[59] T. Liu, P. Li, N. Yao, T. Kong, G. Cheng, S. Chen, W. Luo, Self-sacrificial template-directed vapor-phase growth of MOF assemblies and surface vulcanization for efficient water splitting, Adv. Mater. 31 (21) (2019), 1806672.
[60] P. He, Y. Xie, Y. Dou, J. Zhou, A. Zhou, X. Wei, J.R. Li, Partial sulfurization of a 2D MOF array for highly efficient oxygen evolution reaction, ACS Appl. Mater. Interfaces 11 (44) (2019) 41595–41601.
[61] H. Xu, K. Ye, K. Zhu, J. Yin, J. Yan, G. Wang, D. Cao, Template-directed assembly of urchin-like CoS x/Co-MOF as an efficient bifunctional electrocatalyst for overall water and urea electrolysis, Inorg. Chem. Front. 7 (14) (2020) 2602–2610.
[62] S. Zheng, X. Guo, H. Xue, K. Pan, C. Liu, H. Pang, Facile one-pot generation of metal oxide/hydroxide@ metal–organic framework composites: highly efficient bifunctional electrocatalysts for overall water splitting, Chem. Commun. 55 (73) (2019) 10904–10907.
[63] N. Yao, Z. Fan, R. Meng, H. Jia, W. Luo, A cobalt hydroxide coated metal-organic framework for enhanced water oxidation electrocatalysis, Chem. Eng. J. 408 (2021), 127319.
[64] X. Wang, H. Zhang, Z. Yang, C. Zhang, S. Liu, Ultrasound-treated metal-organic framework with efficient electrocatalytic oxygen evolution activity, Ultrason. Sonochem. 59 (2019), 104714.
[65] S. Zhao, Y. Wang, J. Dong, C.T. He, H. Yin, P. An, Z. Tang, Ultrathin metal–organic framework nanosheets for electrocatalytic oxygen evolution, Nat. Energy 1 (12) (2016) 1–10.